ZANCO Journal of Pure and Applied Sciences

TYPE Original article
DOI http://dx.doi.org/10.21271/ZJPAS.37.6.11

OPEN ACCESS

*Corresponding author

Ghassan M. Werdina
ghassan.werdina@su.edu.krd

RECEIVED :04 /01 /2025
ACCEPTED :18/07/ 2025
PUBLISHED :31/ 12/ 2025

KEYWORDS:
Torsion, Slab, Finite element, Stiffness, Concrete.

Finite Element Analysis of Concrete Slabs Under Torsion

Ghassan M. Werdina[1, *], Omar Q. Aziz[2]

1 Department of Water Resources Engineering, College of Engineering, Salahaddin University-Erbil, Erbil, Kurdistan Region, Iraq
2 Department of Civil Engineering, College of Engineering, Salahaddin University-Erbil, Erbil, Kurdistan Region, Iraq

ABSTRACT

Many researchers have been interested in the study of torsion in concrete members during the last decades. Most of these studies focused on the reinforced beams under torsion and not deeply researched the case of slab. This paper presents a study on the behavior of reinforced concrete slabs under torsion by using finite element analysis (FEA). Twenty-one slabs with different reinforcement and concrete compressive strength have been included in the study. To apply torsional moment on the slabs, vertical displacement at three corners was constrained and the load was applied to the fourth corner. According to the results, steel bar size had more influence on the torsional yielding moment compared to the torsional cracking moment. Using steel bar size of 12 mm instead of 8 mm increased the torsional cracking and yielding moments by 4% and 19% respectively, for the slab with compressive strength of concrete of 50 MPa. Furthermore, both the torsional cracking and yielding moments substantially increased with the increase in compressive strength of concrete. Raising the compressive strength of concrete from 21 MPa to 50 MPa increased the torsional cracking and yielding moments by 54% and 44% respectively. Torsional stiffness of reinforced concrete slabs in the uncracked stage is about 20-28 times that in the cracked stage.

:

1.Introduction

Reinforced concrete slabs are critical in floors, roofs, and bridge decks, yet their design often neglects torsional effects due to analytical complexity. The torsional stiffness, when taken into account, relieves a considerable amount of bending moment. For simply supported square slabs, the exact theory of elastic plates bending shows that 25 percent of bending moment is alleviated due to twisting moment (Nilson et al., 2010). Moreover, the concrete slab torsional stiffness in the cracked stage is considerably less than the stiffness in the elastic stage. To have a safe design of structural concrete members, it is important to take into account the effects of torsion. Therefore, a comprehensive understanding of torsion's impact and familiarity with the design application of analytical models are necessary (ACI 445.1R-12). The current analytical models and design practices often fail to capture the full effects, raising concerns about safety and efficiency in structural design.

Comprehensive research on the torsional response of reinforced concrete members has been conducted over the last three decades (ACI 445.1R-12). Most torsion research focuses on beams, with limited slab studies (Ibraheem and Mukhlif, 2021, Hasan and Taha, 2020, Mawlood et al., 2021), resulting in a significant gap in our understanding of torsional behavior in slab elements. This gap challenges the validity of extrapolating beam-based torsion theories to slabs, risking unsafe designs. Between 1995 and 2015, design engineers shifted from primarily relying on traditional slab analysis methods to adopting finite element analysis (FEA). More recently, engineers use FEA to assist in the two-way members structural design (ACI 447R-18, Yaseen and Ihsan, 2020). Marti and Kong (1987) presented the torsional stiffness analytical solution at pre-cracking and post-cracking stages for the reinforced concrete slab. The reduction in concrete stiffness due to cracking (tensile strain softening) was modeled using empirical stress-strain relationships derived from tests on concrete panels under membrane forces. This reliance on empirical data, while practical, introduces potential inaccuracies that may limit the generalizability of their findings. It was concluded that this softening issue has a significant effect on strength and stiffness, and that a yield-line method may significantly overestimate the torsional resistance. This discrepancy suggests that current design approaches may not fully capture the complex interactions within slab elements, particularly at various stages of cracking and yielding. May et al. (2001) studied the behavior of reinforced concrete elements subjected to bending and twisting moments. Fourteen reinforced concrete slabs, with size of 1.6 m x 1.6 m x 0.15 m, were tested under uniform bending moments, applied about one or both orthogonal axes, with or without the addition of uniform twisting moments. Results of the analysis were compared with the experimental tests. The predictions were found to be non-conservative when the twisting moment was substantial. This highlights a potential limitation in the current modeling approaches, where the complexity of real-world loading conditions may not be fully captured, and the need for more robust modeling techniques. Lopes et al. (2013) studied the response of concrete slabs under torsion, focusing on the stiffness of both the cracked and uncracked stages. The experimental study involved nine reinforced concrete slabs under pure torsion, six slabs with sizes of 2.1 m x 2.1 m x 0.15 m, and three slabs with sizes of 2.8 m x 2.8 m x 0.15 m. It was found that the ratio of torsional stiffness in the cracked stage, to that of the elastic stage was about 1/17–1/15. Nguyen et al. (2016) conducted an experimental research on the torsional stiffness of concrete slabs. They tested seven slabs, each measuring 1.9 m x 1.9 m, subjected to torsional loading. The study found three phases of behavior, that included the concrete pre-cracking and post-cracking, and the steel post-yielding. Greater slab thickness resulted to have more torsional stiffness, since reinforcement were located farther from middle plane. The influences of reinforcement on the torsional stiffness was negligible in the stage before concrete cracking. After concrete cracking, the torsional stiffness decreased very fast, and became very small compared to torsional stiffness before cracking. The effect of reinforcement in this stage was clear and

significant. Nguyen and Pham (2017) investigated the reinforced concrete slab subjected to torsion, using the finite element analysis and experimental tests. The experimental tests included three concrete slabs measuring 1.9 m x 1.9 m x 0.15 m. The response of slabs during the pre-cracking and post-cracking phases of concrete was examined. Torsional stiffness during the stage after cracking of concrete and yielding of steel was 1/25 of the stiffness in pre-cracking stage. This variation in stiffness results among different researchers highlights the need for further investigation in this field. Ibraheem and Mukhlif (2021) experimentally investigated nine reinforced concrete slabs under pure torsion. The slabs had a length of 800 mm and thickness of 50 mm, with three different widths of 400 mm, 500 mm, and 600 mm. They concluded that the slab width and reinforcement ratio had more influence on the slab stiffness, strength, and ductility. However, the limited scope of this study, focusing primarily on specific geometric and material properties, suggests that further research is needed to fully understand the broader implications of torsion on different slab configurations and materials.

This study provides a comprehensive numerical analysis of reinforced concrete slabs under torsion, addressing key knowledge gaps in slab design under torsional loading. Unlike prior research that mainly focuses on beams, this study systematically evaluates the effect of reinforcement bar size and concrete compressive strength on the torsional behavior of slabs. A key novelty of this study lies in its refined numerical methodology, which employs an optimized Concrete Damage Plasticity (CDP) model and a detailed parametric analysis to capture post-cracking and post-yielding slab behavior more accurately. By extending the analysis across a broader range of parameters than previous studies, the findings provide critical insights into stiffness degradation and torsional capacity, contributing to the refinement of design codes. Additionally, the study highlights the limitations of current design approaches in predicting torsional resistance, offering recommendations that could improve the reliability of slab designs in practical applications such as bridge decks and reinforced concrete diaphragms.

2. Problem Statement

This paper studies numerically the influence of concrete compressive strength and reinforcement bar size on the torsional behavior and stiffness of reinforced concrete slabs subjected to torsion. Previous research has not fully explored the combined impact of these factors, particularly in the context of finite element analysis. By addressing this gap, the present study provides a clearer understanding of the influence of torsion on concrete slabs, which is crucial for the safe and cost-effective design of reinforced concrete members.

3. Research Methodology

This study numerically analyzes the torsional behavior of reinforced concrete slabs using 3D solid element in ABAQUS software. Non-linear finite element analysis is utilized to get an in-depth understanding of the loads, torsional stiffness, twisting moment-rotation relationship at different stages for the reinforced concrete slab under torsion.

4. Study specimens and variables

The study includes finite element analysis for twenty-one square slabs measuring 2.8 m x 2.8 m x 0.15 m. The slab dimensions were chosen to align with previous experimental studies for comparison purposes, and to ensure a representative size for real-world structural applications such as bridge decks and floor slabs. As shown in **Figure 1**, all slabs were reinforced with two orthogonal layers of steel bars, placed at both the top and bottom surfaces, with bars spaced at 100 mm in each direction. The reinforcement was designed to provide a realistic representation of typical slab reinforcement practices while ensuring sufficient flexural and torsional capacity. The yield strength of the steel bars (f_y) is 542 MPa for all slabs. Variables of the study include the compressive strength of concrete and the steel bar size. The study includes seven groups of slabs with varying concrete compressive strength that ranges from 21 MPa to 50 MPa. Every group includes three different reinforcement bar size (8 mm, 10 mm and 12 mm). Table 1 presents the details of the study specimens and variables.

5. Numerical finite element analysis of the slabs

In the current study, numerical simulation is performed by using ABAQUS which is a software capable to solve a broad range of nonlinear and linear problems.

5.1 Geometric Modeling and Bounday Conditions

The initial step was to input the geometry of the slabs in ABAQUS/Explicit model. Concrete slabs and support plates were modeled using 3D solid elements. Deformable “wire” type part was used to define the reinforcement.

Table 1. Details of the Specimens and Variables

Group No.	Specimen No.	f'_c (MPa)	Reinforcement bar size (mm)	Reinforcement ratio ρ [a]	ρ/ρ_b
G21	S-21-8	21	8	0.004	0.27
	S-21-10	21	10	0.0063	0.43
	S-21-12	21	12	0.0091	0.62
G25	S-25-8	25	8	0.004	0.23
	S-25-10	25	10	0.0063	0.36
	S-25-12	25	12	0.0091	0.52
G30	S-30-8	30	8	0.004	0.19
	S-30-10	30	10	0.0063	0.30
	S-30-12	30	12	0.0091	0.43
G35	S-35-8	35	8	0.004	0.16
	S-35-10	35	10	0.0063	0.26
	S-35-12	35	12	0.0091	0.37
G40	S-40-8	40	8	0.004	0.14
	S-40-10	40	10	0.0063	0.23
	S-40-12	40	12	0.0091	0.33
G45	S-45-8	45	8	0.004	0.13
	S-45-10	45	10	0.0063	0.20
	S-45-12	45	12	0.0091	0.29
G50	S-50-8	50	8	0.004	0.11
	S-50-10	50	10	0.0063	0.18
	S-50-12	50	12	0.0091	0.26

[a] Both the compression and tension faces have the same reinforcement ratio.

As illustrated in **Figure 1**, the reactions act vertically. Supports were placed to prevent the downward movement at corners C3 and C4, while at C2 the support was placed to restrict the vertical upward movement. At corner C1, a vertical downward load was applied, ensuring accurate torsional response representation (Lopes et al., 2013, Nguyen and Pham, 2017, Nguyen et al., 2016). Additionally, steel plates were placed at the load application and support points to ensure uniform stress distribution. The load was subjected as a specified vertical displacement using smooth step amplitude function. The analysis was applied in step-1 (Dynamic, Explicit), that was after the initial step.

5.2 Material Modeling

After completing the geometry input, slabs material properties had to be input in ABAQUS. This process is detailed in the following sub-sections.

A. Concrete: To describe the response of concrete under loading, the Concrete Damage Plasticity (CDP) model, which is provided in ABAQUS, was utilized. The Concrete Damage Plasticity (CDP)

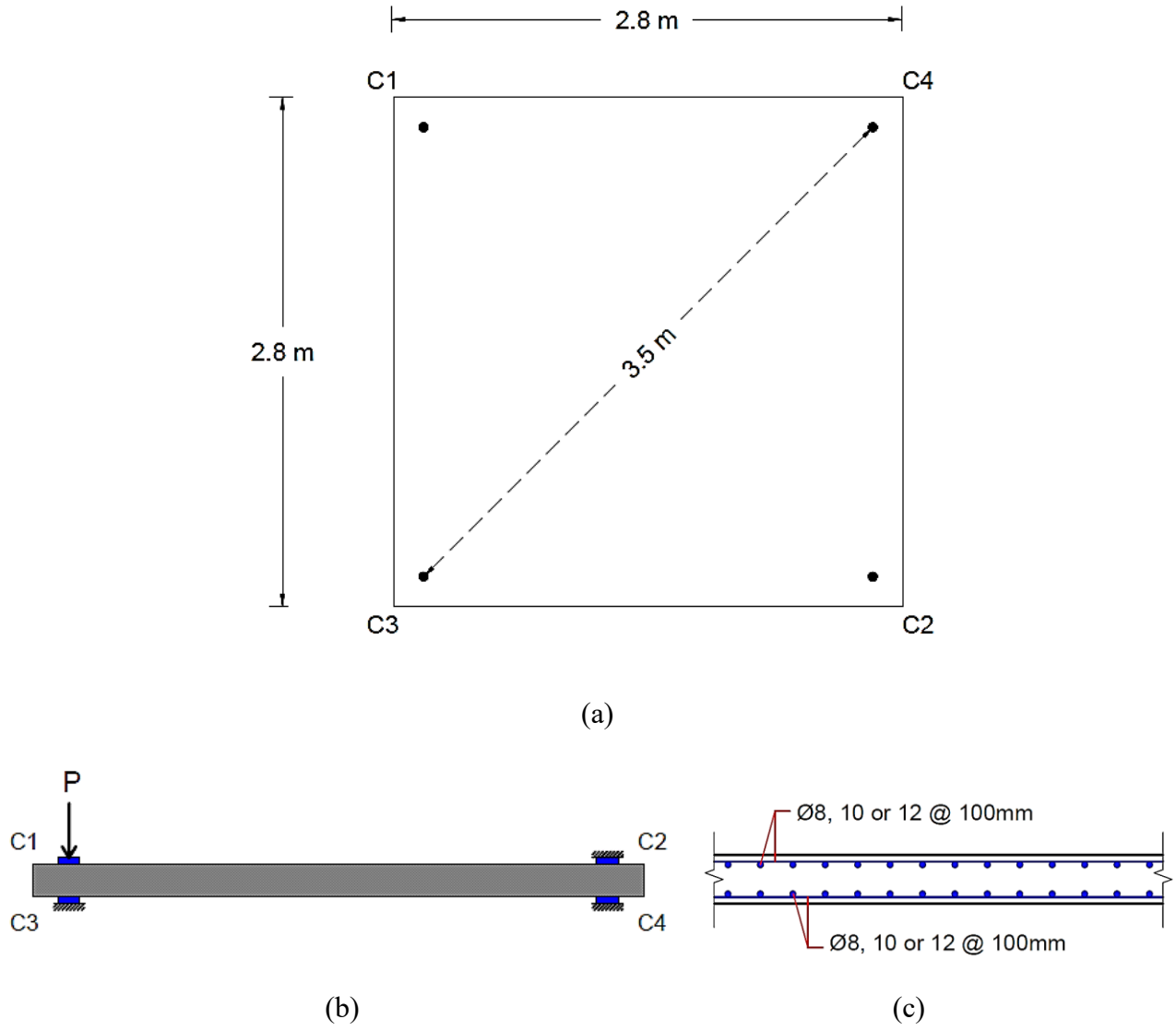

Figure 1. Boundary conditions and reinforcement of the slabs: (a) Dimensions and supports, (b) Setup and supports, (c) Reinforcement of the slabs

model considers the concrete degradation and identifies two failure modes, that are crushing under uniaxial compression and cracking under uniaxial tension. Several parameters are needed to specify the concrete's plasticity model, that include the plastic potential eccentricity, the dilation angle (ψ), the shape factor of the yielding surface, the ratio of stresses in compression in biaxial to uniaxial states (fbo / fco), and the viscosity parameter. The CDP parameters for this study are presented in Table 2 (Dere and Koroglu, 2017, DSS, 2012, Esfahani et al., 2017).

The following equation, proposed by Saenz (1964), is used to define the concrete stress-strain relationship under uniaxial compression:

$$\sigma_c = \frac{E_c \varepsilon_c}{1+(R+R_E-2)\left(\frac{\varepsilon_c}{\varepsilon_0}\right)-(2R-1)\left(\frac{\varepsilon_c}{\varepsilon_0}\right)^2+R\left(\frac{\varepsilon_c}{\varepsilon_0}\right)^3} \quad (1a)$$

$$R = \frac{R_E(R_\sigma-1)}{(R_\varepsilon-1)^2} - \frac{1}{R_\varepsilon} \quad (1b)$$

$$R_E = \frac{E_c}{E_0} \quad (1c)$$

$$E_0 = \frac{f_c'}{\varepsilon_0} \quad (1d)$$

values of Rε=4 and Rσ=4 are applicable, σ_c represents the effective stress, ε_c is the effective

strain, ε_0 is the strain of concrete at ultimate stress and was assumed to be 0.003, and E_c is the initial elasticity modulus.

Table 2. CDP Parameters

CDP parameters	Value
K	0.667
Eccentricity	0.1
Dilation angle (ψ)	31°
biaxial/uniaxial ratio (fbo / fco)	1.16
Viscosity parameter	0
Poisson's ratio	0.18

For the concrete stress-strain relationship in tension, the following equations have been used (Belarbi and Hsu, 1994, Hsu and Mo, 2010, Tamai, 1988, Wang and Hsu, 2001):

$$\sigma_t = E_c \varepsilon_t \quad \text{for} \quad \varepsilon_t \leq \varepsilon_{cr} \tag{2a}$$

$$\sigma_t = f_t \left(\frac{\varepsilon_{cr}}{\varepsilon_t}\right)^{0.4} \quad \text{for} \quad \varepsilon_t > \varepsilon_{cr} \tag{2b}$$

$$\boldsymbol{f_t = 0.31\sqrt{f'_c}} \tag{3b}$$

where ε_{cr} is the concrete tensile strain at ultimate stress, which was taken as 0.00015, ε_t is the tensile strain of concrete, and f_t is the concrete tensile peak stress.

Concrete degradation is determined by the damage parameter in compression (*dc*), and the damage parameter in tension (*dt*). In this study, *dc* is defined as the ratio of the compressive stress of concrete after crushing to the stress at initial yield, and *dt* is calculated as the ratio of the tensile stress of concrete beyond cracking to the peak tensile stress (Esfahani et al., 2017). Additionally, a value of 0.8 was assumed for the stiffness recovery factor in compression (w_c), indicating that this stiffness is largely restored as cracks close when the load shifts from tension to compression. Conversely, a value of 0.0 was assumed for the stiffness recovery factor in tension (w_t), reflecting that this stiffness does not recover when the load shifts from compression to tension after concrete crushing has begun.

B. Reinforcement: The model of linear elastic-perfect plastic response was used for the reinforcement material properties, with a value of 200 GPa for the modulus of elasticity. The steel bars were simulated to be embedded in the concrete.

C. Plates: The model of linear elastic response was used for the plate material properties, with a value of 200 GPa for the modulus of elasticity. The type of "Tie constraints" was used as the interaction between the concrete and plates.

5.3 Element Types and Mesh Generation

As shown in **Figure 2,** the first order hexahedral elements were used to mesh the solid members. These are eight nodes bricks, reduced integration (C3D8R), that provide good results for minimum cost in 3D analyses. For the steel bars, a 3D truss elements (T3D2) were used. The elements general size was 100 mm.

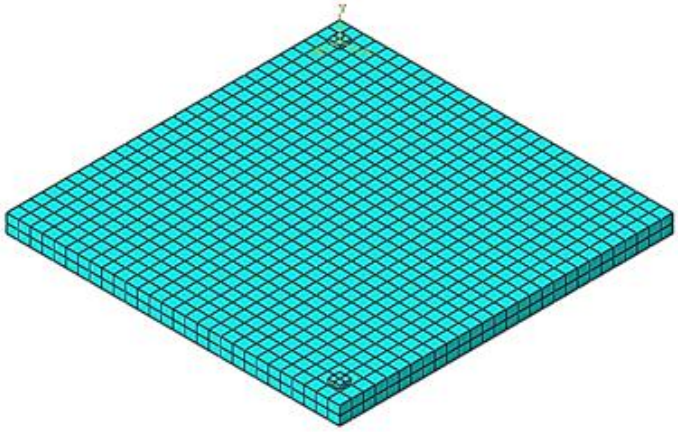

Figure 2. Elements and Meshing

6. Results

6.1 Load-Displacement Relationship

As presented in Table 3, the load-displacement relationship was established for all specimens. The information presented include the cracking load (P_{cr}) and the cracking displacement (d_{cr}), the yielding load (P_y) and the yielding displacement (d_y), stage I stiffness (K_I), stage II stiffness (K_{II}) and the ratio of the stiffness in these two stages. K_I is the stiffness at the stage before the slab cracking, and K_{II} is the slope of the tangent at cracking stage. **Figure 3** shows that point (P_y, d_y) is the last point in stage II and correspond to the onset of yielding of the steel. This point is identified by the intersection of a horizontal line from the point of ultimate load and the line

corresponds to stage II (Lopes et al., 2013). The *P-d* relationships for all slabs are shown in **Figure 4** and **Figure 5**. The measured displacement in these figures is for the free corner of the slab. These curves exhibit similar trends across the different slabs. Cracking load value increased with the rise in concrete compressive strength. It increased 54% by increasing the *f'c* from 21 MPa to 50 MPa. The cracking load value increased only 4% when 12 mm steel bars were used instead of 8 mm, aligning with the findings of Ibraheem and Mukhlif (2021), who also reported a limited effect of steel reinforcement on the cracking load. Maximum increase of P_y as effect of steel bar was 19% (from 64.9 kN for S-50-8 to 77.1 kN for S-50-12) as the steel bar was increased from 8 mm to 12 mm, for slab with concrete compressive strength of 50 MPa. The value of P_y increased 44% (from 53.6 kN for S-21-12 to 77.1 kN for S-50-12) when the compressive strength of concrete raised from 21 MPa to 50 MPa. The value of the stiffness in stage I is more than that in stage II and the maximum ratio of K_I/K_{II} is 28.1.

Table 3. Load and Displacement Results

Specimen No.	P_{cr} (kN)	d_{cr} (mm)	P_y (kN)	d_y (mm)	K_I (kN/m)	K_{II} (kN/m)	K_I/K_{II}
S-21-8	23.6	10.64	49.8	275.05	2216	99	22.4
S-21-10	24.1	10.64	52.1	286.50	2267	101	22.4
S-21-12	24.6	10.64	53.6	270.95	2314	111	20.8
S-25-8	25.9	10.64	52.5	266.33	2434	104	23.4
S-25-10	26.5	10.64	55.8	266.46	2489	115	21.7
S-25-12	27.0	10.64	57.2	249.96	2534	126	20.1
S-30-8	28.3	10.64	57.8	272.48	2661	113	23.6
S-30-10	29.0	10.64	61	284.34	2729	117	23.4
S-30-12	29.5	10.64	63.4	268.31	2770	132	21.0
S-35-8	30.5	10.64	58.5	272.52	2862	107	26.7
S-35-10	31.1	10.64	64.8	295.29	2920	118	24.7
S-35-12	31.7	10.64	66.1	269.79	2980	133	22.5
S-40-8	32.6	10.64	61.1	267.37	3063	111	27.6
S-40-10	33.2	10.64	70.2	298.97	3123	128	24.4
S-40-12	33.9	10.64	70	272.52	3184	138	23.1
S-45-8	34.4	10.64	63.5	264.68	3228	115	28.1
S-45-10	35.2	10.64	73	302.78	3303	130	25.5
S-45-12	35.8	10.64	74.2	269.19	3361	149	22.6
S-50-8	36.2	10.64	64.9	238.19	3403	126	27.0
S-50-10	36.9	10.64	73	274.31	3469	137	25.4
S-50-12	37.6	10.64	77.1	271.74	3537	151	23.4

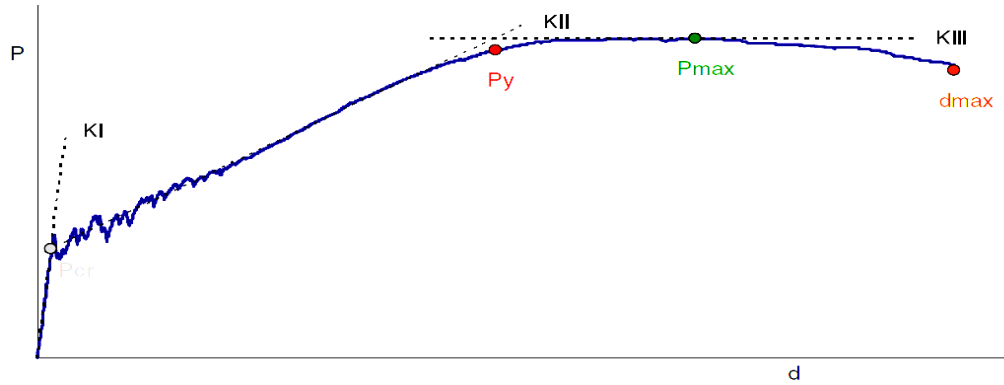

Figure 3. The main points in *P-d* curve Reproduced with permission from Lopes et al., 2013, Materials and Structures, 47. This material is not part of the Open Access license of this article.

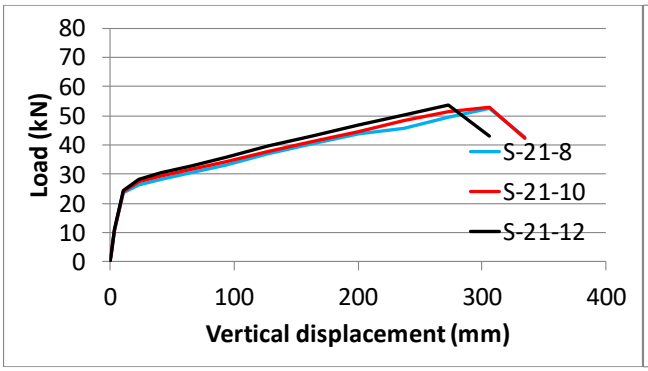

(a) *f'c*=21 MPa

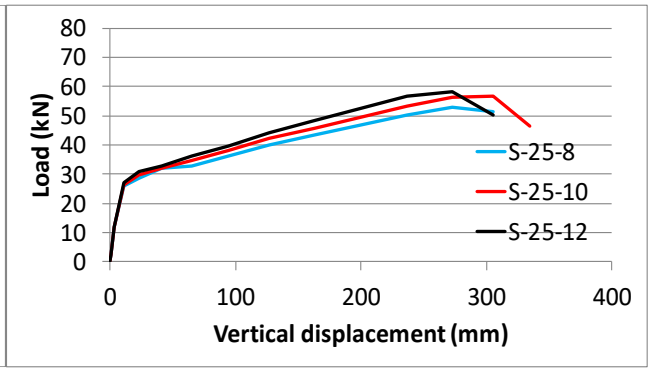

(b) *f'c*=25 MPa

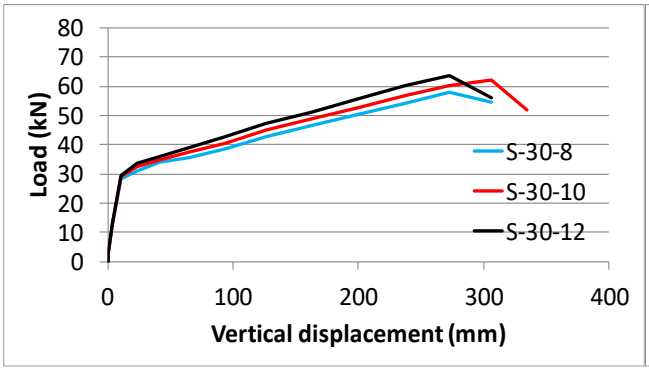

(c) *f'c*=30 MPa

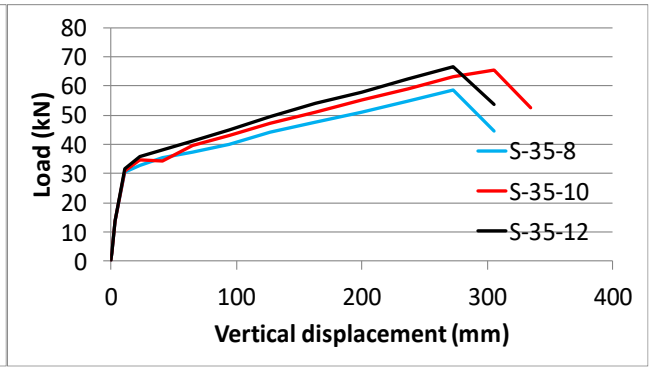

(d) *f'c*=35 MPa

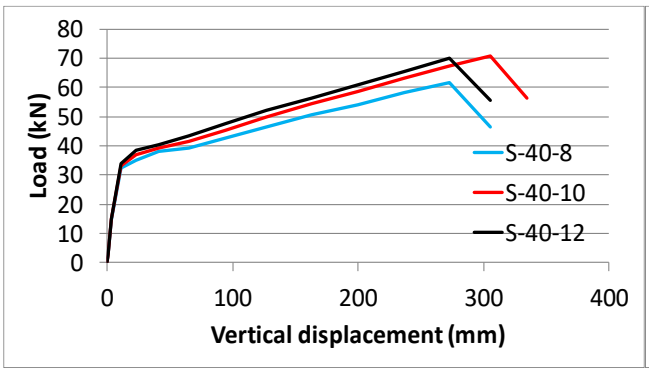

(e) *f'c*=40 MPa

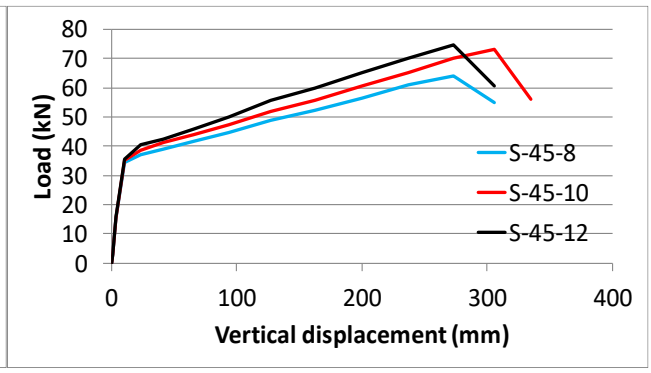

(f) *f'c*=45 MPa

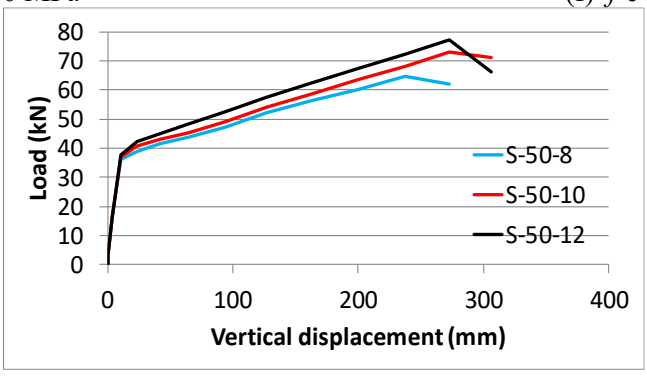

(g) *f'c*=50 MPa

Figure 4. *P-d* curves of the slabs for different *f'c*

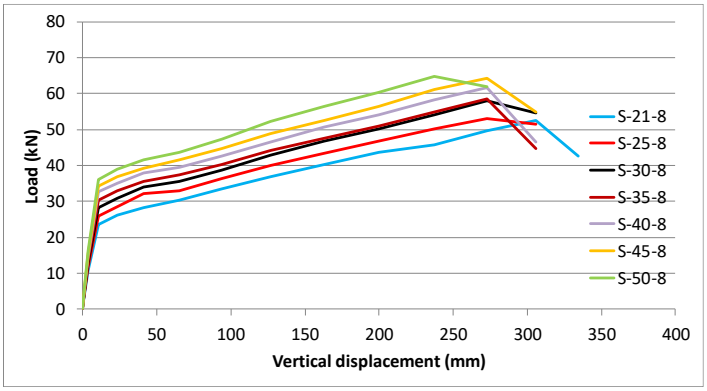

(a) Bar diameter=8 mm

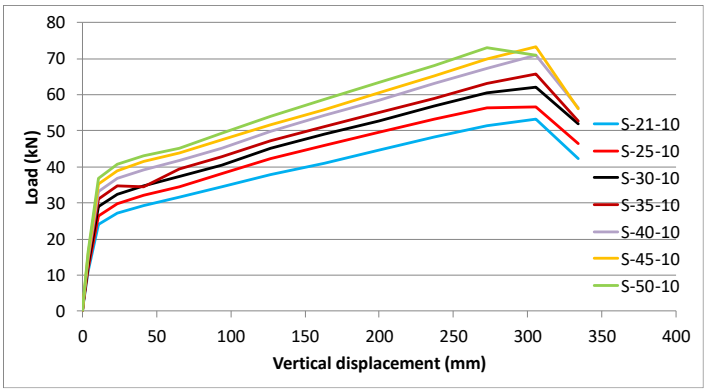

(b) Bar diameter=10 mm

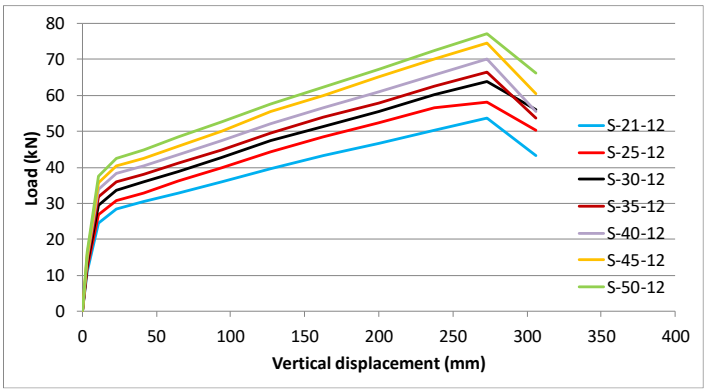

(c) Bar diameter=12 mm

Figure 5. *P-d* curves of the slabs for different bar diameter

6.2 Torsional Moment-Rotation Relationship

This section demonstrates the torsional moment-rotation relationship. The following equation is used to determine the torsional moment (T) (Nguyen et al., 2016):

$$T = m_{xy} = (\frac{P}{2} + \frac{W}{8})\frac{l}{b} \quad (3)$$

where T or m_{xy} is the slab average torsional moment, W is the slab self weight, P is the load in corner C1, l is the lever arm of the subjected load (2.475 m) and b=2.8 m. The following equation is used to determine the rotation per unit length (θ) of the slab (Lopes et al., 2013):

$$\theta = \frac{d}{(L.cos45°)^2} \quad (4)$$

where L is the slab diagonal length (3.5 m).

Table 4 illustrates the torsional cracking moment (T_{cr}) and the corresponding cracking rotation (θ_{cr}), the torsional yielding moment (T_y) and the corresponding yielding rotation (θ_y), stage I torsional stiffness (K_{TI}), stage II torsional stiffness (K_{TII}) and the ratio of the stiffness in these two stages. The following equations (Lopes et al., 2013) were used to determine the torsional stiffness:

$$K_{TI} = \frac{T_{cr}}{\theta_{cr}} \quad (5)$$

$$K_{TII} = \frac{T_y - T_{cr}}{\theta_y - \theta_{cr}} \quad (6)$$

Torsional cracking moment slightly increased with the increase in steel bar size. It increased only 4% as the bar size increased from 8mm to 12 mm. While the increase in torsional cracking moment was more by increasing concrete compressive strength, as it raised 54% by increasing *f'c* from 21 MPa to 50 MPa. Steel bar size had more effect on T_y than T_{cr}. Maximum increase in T_y as the effect of steel bar was 19% (from 28.7 kN.m/m for S-50-8 to 34.1 kN.m/m for S-50-12) when the steel bar 12 mm was used instead of 8 mm for the slab with concrete compressive strength of 50 MPa. Meanwhile, T_y increased 44% (from 23.7 kN.m/m for S-21-12 to 34.1 kN.m/m for S-50-12) when the compressive strength of concrete increased from 21 MPa to 50 MPa. Stage I torsional stiffness is substantially higher than the stage II torsional stiffness, and the value of K_{TI}/K_{TII} ranges between 20.1 and 28.1. Results of the torsional stiffness were compared with the experimental investigation of Lopes et al. (2013). This comparison focused on the group of slabs in Table 4 with a compressive strength of concert (*f'c*) between 25 MPa and 35 MPa, matching the *f'c* range of the referenced experimental study. The average values of K_{TI}, K_{TII}, and K_{TI}/K_{TII} in the present study were 7332 kN/m, 320 kN/m, and

23, respectively. In the Lopes et al. study (excluding slabs with edge reinforcement), the average values were 6844 kN/m, 372 kN/m, and 19, respectively, indicating that the results of both studies are closely aligned. Additionally, the K_{TI}/K_{TII} ratio reported by Nguyen and Pham (2017) was 25, which is also very close to the present study results.

T-θ relationships for slabs are shown in **Figure 6** and **Figure 7**. These curves are comparable across the different slabs, showing a raise in the torsional stiffness in stage II with the increase in bar size and concrete compressive strength. Consistent with the experimental investigations by Ibraheem and Mukhlif (2021) and Lopes et al. (2013), three distinct stages can be identified in these curves. The first phase is the elastic stage prior to cracking, followed by a second stage after cracking, marked by a reduced slope of curves. The softening phase is the third stage that occurs past the maximum torsional moment. Graphs with reduced reinforcement exhibit less slope after cracking, aligning with the Peng and Wong (2011) results, who observed that reduced reinforcement levels led to a greater increase in steel strains and, consequently, larger twist angles upon initial cracking. Ibraheem and Mukhlif (2021) also reported similar trends in their curves.

Table 4. Torsional Moment and Rotation Results

Specimen No.	T_{cr} (kN.m/m)	θ_{cr} (rad/m)	T_y (kN.m/m)	θ_y (rad/m)	K_{TI} (kN/rad/m)	K_{TII} (kN/rad/m)	K_{TI}/K_{TII}
S-21-8	10.4	0.0017	22.0	0.0449	6000	268	22.4
S-21-10	10.7	0.0017	23.0	0.0468	6137	274	22.4
S-21-12	10.9	0.0017	23.7	0.0442	6264	301	20.8
S-25-8	11.4	0.0017	23.2	0.0435	6589	282	23.4
S-25-10	11.7	0.0017	24.7	0.0435	6738	310	21.7
S-25-12	11.9	0.0017	25.3	0.0408	6860	342	20.1
S-30-8	12.5	0.0017	25.5	0.0445	7203	305	23.6
S-30-10	12.8	0.0017	27.0	0.0464	7386	316	23.4
S-30-12	13.0	0.0017	28.0	0.0438	7498	356	21.0
S-35-8	13.5	0.0017	25.9	0.0445	7748	290	26.7
S-35-10	13.7	0.0017	28.6	0.0482	7905	321	24.7
S-35-12	14.0	0.0017	29.2	0.0440	8066	359	22.5
S-40-8	14.4	0.0017	27.0	0.0437	8290	301	27.6
S-40-10	14.7	0.0017	31.0	0.0488	8455	347	24.4
S-40-12	15.0	0.0017	30.9	0.0445	8620	373	23.1
S-45-8	15.2	0.0017	28.1	0.0432	8738	311	28.1
S-45-10	15.5	0.0017	32.3	0.0494	8940	351	25.5
S-45-12	15.8	0.0017	32.8	0.0439	9099	402	22.6
S-50-8	16.0	0.0017	28.7	0.0389	9212	341	27.0
S-50-10	16.3	0.0017	32.3	0.0448	9391	370	25.4
S-50-12	16.6	0.0017	34.1	0.0444	9574	409	23.4

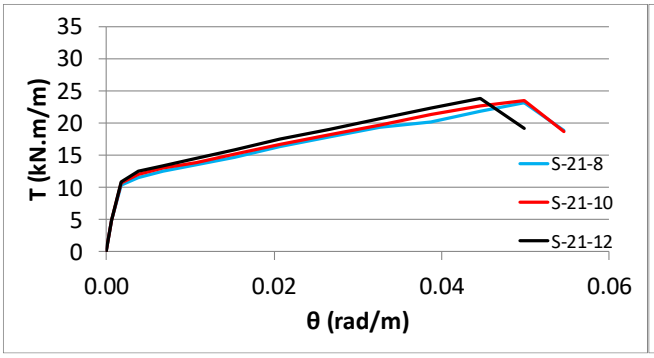

(a) $f'c$=21 MPa

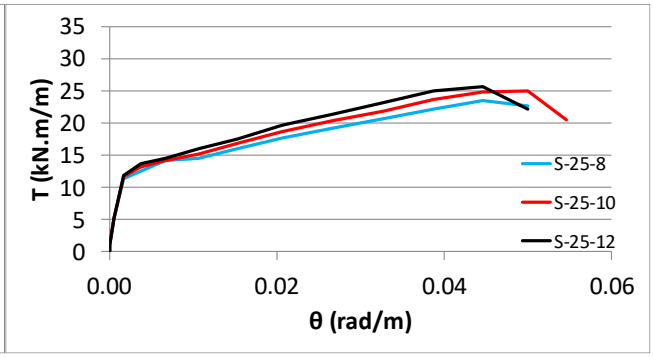

(b) $f'c$=25 MPa

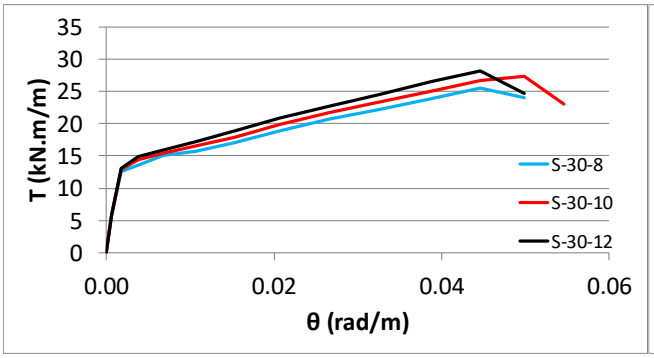

(c) $f'c$=30 MPa

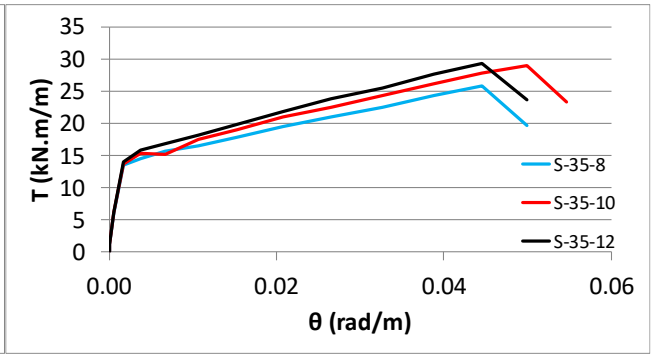

(d) $f'c$=35 MPa

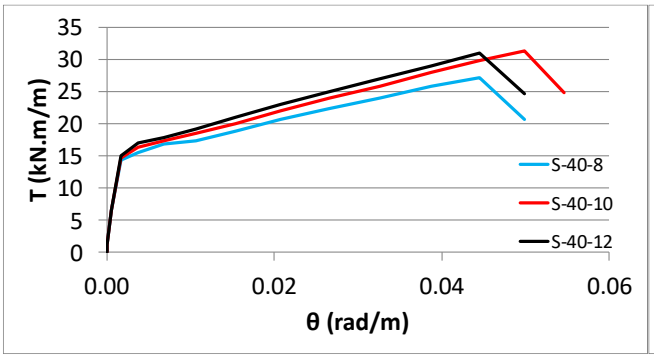

(e) $f'c$=40 MPa

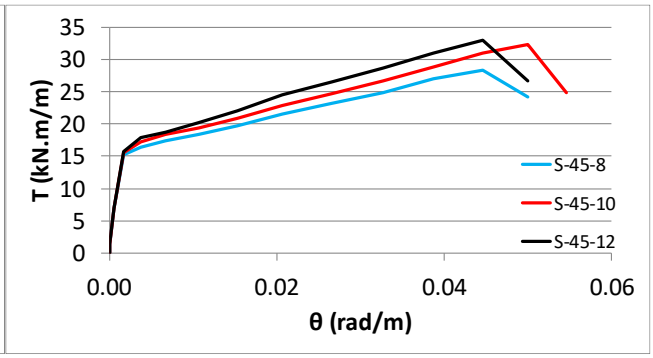

(f) $f'c$=45 MPa

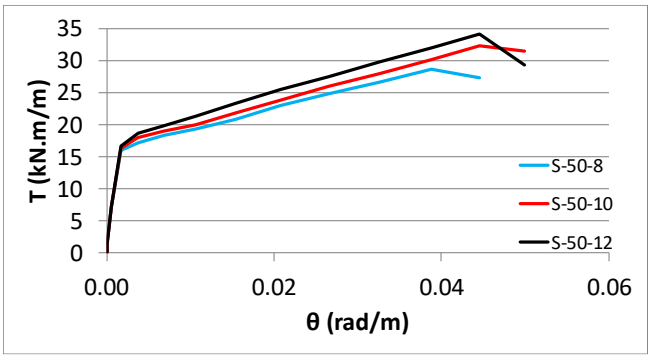

(g) $f'c$=50 MPa

Figure 6. T-θ curves of the slabs for differernt $f'c$

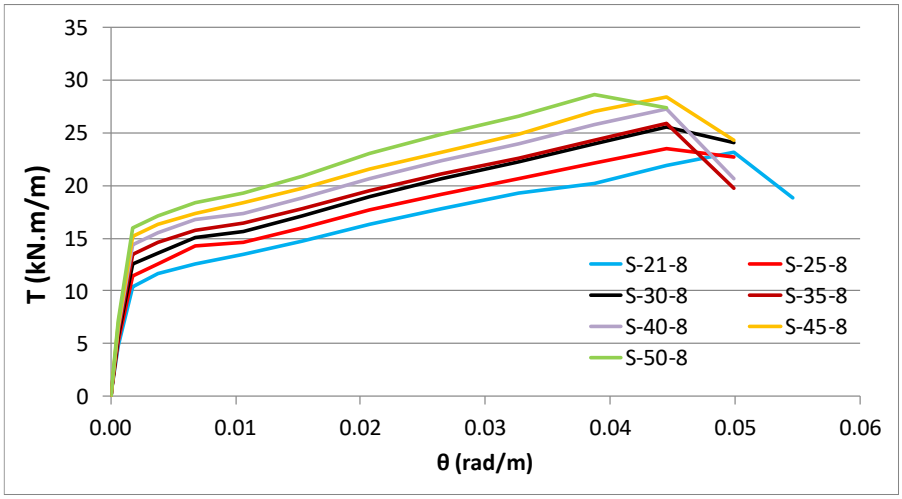

(a) Bar diameter=8 mm

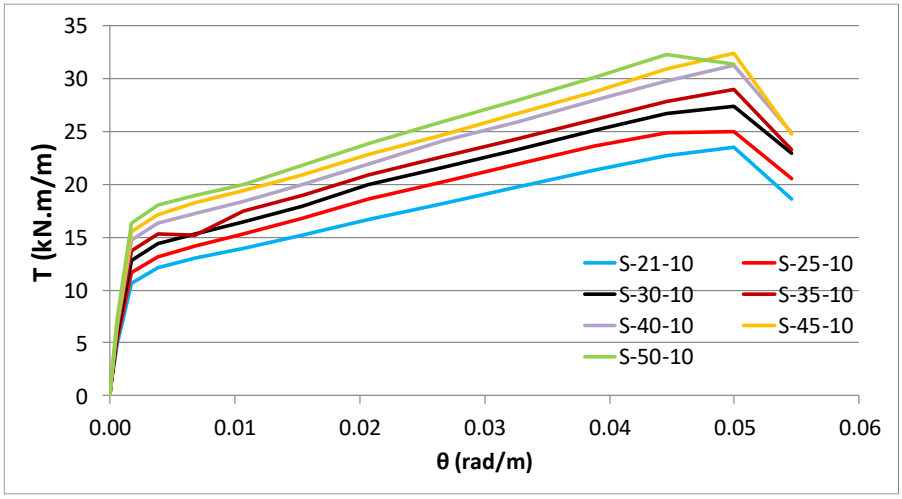

(b) Bar diameter=10 mm

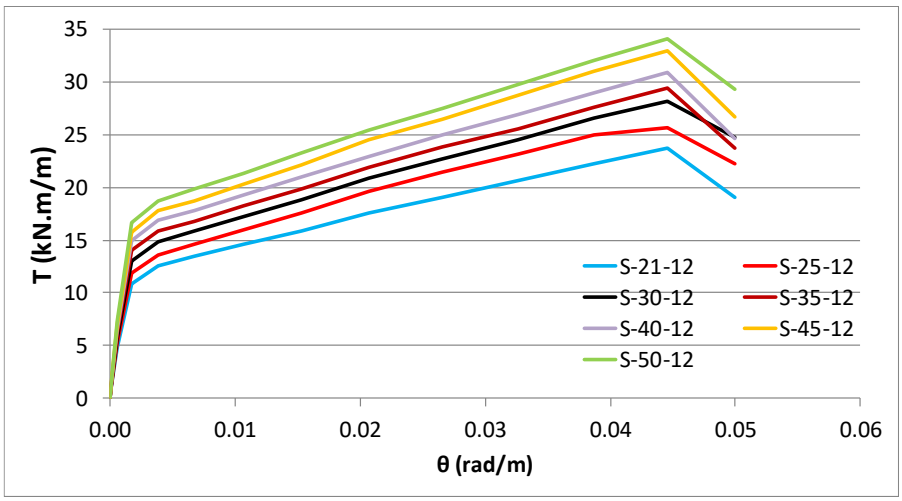

(c) Bar diameter=12 mm

Figure 7. T-*θ* curves of the slabs for different bar diameter

6.3 Sensitivity Analysis

To ensure the accuracy and stability of the numerical model, a mesh sensitivity analysis was conducted for a typical slab (S-40-10) using four different mesh sizes: 120 mm, 100 mm, 80 mm, and 60 mm. The results demonstrated that as the mesh was refined from 100 mm to 60 mm, the solution remained stable, indicating numerical convergence. However, the 120 mm mesh exhibited irregular behavior, suggesting that it was too coarse to capture the slab's response accurately. Based on this assessment, the 100 mm mesh was selected as it provided stable and convergent results while maintaining computational efficiency. The comparison of mesh refinement effects is illustrated in **Figure 8**.

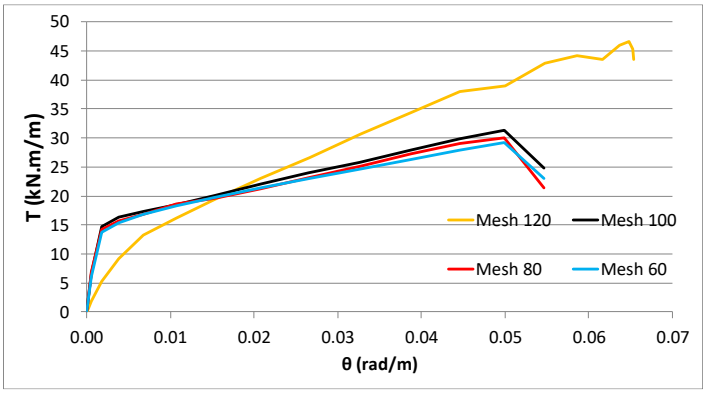

Figure 8. Sensitivity analysis results

6.4 Verification of the FEA Model

To verify the FEA model and measure its accuracy, the results of the slab S-30-8 were compared with the experimental results of two slabs, obtained from the *P-d* relationship curves of Lopes et al. (2013) These two slabs have the same dimensions, supports and reinforcement of the slab S-30-8 included in the current FEA analysis, and the results are presented in Table 5. The comparison included the maximum applied load P_{max} and the vertical displacement at this load (d_{pmax}). As shown in Table 5, the current study results are very close to that of the experimental study of Lopes et al. P_{max} of the current study is 57.9 kN representing 105.3% of the average P_{max} of the two slabs of Lopes et al. experimental study (55 kN). Similarly, the d_{pmax} of the current study is 273 mm representing 99.3% of the average d_{pmax} of the two slabs of Lopes et al. (275 mm).

In addition to verification with Lopes et al., further validation was conducted by comparing key results mentioned in section 6.1 and 6.2 with experimental studies. The limited effect of reinforcement size on cracking load aligns with Ibraheem and Mukhlif (2021), while post-cracking behavior trends are consistent with Peng and Wong (2011) and Ibraheem and Mukhlif (2021). Similarly, the torsional stiffness values from this study closely match those reported by Lopes et al. (2013) and Nguyen and Pham (2017). Consistent with the experimental findings of Ibraheem and Mukhlif (2021) and Lopes et al. (2013), the torque-twist response follows three stages: an initial elastic phase, a reduced slope after cracking, and a final softening stage, mirroring trends observed in experimental curves. While these comparisons provide confidence in the model's accuracy, broader validation with additional experimental datasets could further strengthen credibility. However, the limited availability of relevant studies on reinforced concrete slabs under torsion restricts direct comparisons.

To further ensure the reliability of the finite element model, potential sources of error and the measures taken to minimize them are discussed below. Several factors can influence the accuracy of the finite element model, including mesh discretization, material modeling assumptions, and boundary conditions. To minimize these errors, a convergence study was conducted to ensure an optimal mesh density, balancing accuracy and computational efficiency. Additionally, the Concrete Damage Plasticity (CDP) model parameters were carefully calibrated based on experimental stress-strain relationships of concrete to ensure realistic material behavior. The boundary conditions and loading application were also refined to closely replicate the experimental setup. Despite these precautions, minor discrepancies in peak torque values may arise due to the idealized assumptions inherent in numerical modeling.

Table 5. Experimental and FEA Results of the Slabs

Study	Specimen No.	P_{max} (kN)	d_{pmax} (mm)
Lopes et al.	S3.5-8-L-N(1)	58	315
	S3.5-8-L-N(2)	52	235
	Average	55	275
Curent	S-30-8	57.9	273
Current/Lopes et al. %		105.3%	99.3%

7. Conclusions

The finite element analysis of twenty-one slabs under torsion yielded a fundamental understanding of their behavior, leading to the following key conclusions:

- Rebar size had minimal impact on cracking resistance (4% increase for 12 mm vs. 8 mm bars).
- Torsional cracking moment increased 54% as the compressive strength of concrete increased from 21 MPa to 50 MPa.
- Steel bar size had more effect on torsional yielding moment (T_y) than torsional cracking moment. Maximum increase in T_y as the effect of steel bar was 19% when the steel bar size increased from 8 mm to 12 mm for the slab with concrete compressive strength of 50 MPa.
- T_y increased 44% by increasing the compressive strength of concrete from 21 MPa to 50 MPa.
- Stage I torsional stiffness was much greater than the stage II value, and the ratio of K_{TI}/K_{TII} ranged between 20.1 and 28.1.
- The T-θ relationship universally exhibited three phases: elastic, post-cracking, and softening. Stiffness in phase II rose with both rebar size and concrete compressive strength.

8. Limitations of the Study

This study offers valuable perspectives on the behavior of reinforced concrete slabs subjected to torsion, but there are several key limitations to consider:

- The study examines only three specific reinforcement bar sizes (8 mm, 10 mm, and 12 mm). Other reinforcement configurations and sizes were not considered, which might affect the extension of these findings to a broader range of applications.
- The range of concrete compressive strengths investigated (21 MPa to 50 MPa) may not encompass all practical applications, particularly for the high strength concretes.

Despite these limitations, the results of this study provide practical insights for optimizing the torsional resistance of concrete slabs. Since existing design codes provide limited guidance on slab torsion, these findings can aid in refining design methodologies and supplementing future code provisions.

Acknowledgment

This research was funded solely by the authors.

Conflict of interest

None

References

ACI 2013. Report on Torsion in Structural Concrete (ACI 445.1R-12). USA: American Concrete Institute.

ACI 2018. Design Guide for Twisting Moments in Slabs (ACI 447R-18). USA: American Concrete Institute.

BELARBI, A. & HSU, T. 1994. Constitutive laws of concrete in tension and reinforcing bars stiffened by concrete. *Structural Journal,* 91**,** 465-474.

DERE, Y. & KOROGLU, M. 2017. Nonlinear FE modeling of reinforced concrete. *International Journal of Structural Engineering Research,* 6**,** 71-74.

DSS 2012. ABAQUS (6.12) Verification Manual. USA: Dassault Systems Simulia Corp.

ESFAHANI, M., HEJAZI, F. & VAGHEI, R. 2017. Simplified damage plasticity model for concrete. *Structural Engineering International,* 27**,** 68-78.

HASAN, S. & TAHA, B. 2020. Aspect ratio consideration in flat plate concrete slab deflection. *ZANCO Journal of Pure and Applied Sciences,* 32**,** 62-77.

HSU, T. & MO, Y. 2010. *Unified theory of concrete structures,* UK, John Wiley and Sons Ltd publication.

IBRAHEEM, O. & MUKHLIF, O. 2021. Behavior of reinforced concrete plates under pure torsion. *Tikrit Journal of Engineering Sciences,* 28**,** 84-97.

LOPES, A., LOPES, S. & CARMO, R. 2013. Stiffness of reinforced concrete slabs subjected to torsion. *Materials and Structures,* 47**,** 227-238.

MARTI, P. & KONG, K. 1987. Response of reinforced concrete slab elements to torsion. *Journal of Structural Engineering,* 113**,** 976-993.

MAWLOOD, B., MOHAMMAD, A., ABDULRAZZAQ, N. & ISMAIL, K. 2021. Shear strength of reinforced high-performance concrete wide beams. *ZANCO Journal of Pure and Applied Sciences,* 33**,** 117-127.

MAY, I., MONTAGUE, P., SAMAD, A., LODI, S. & FRASER, A. 2001. The behaviour of reinforced concrete elements subject to bending and twisting moments. *Structures and Buildings,* 146**,** 161-171.

NGUYEN, M. & PHAM, P. 2017. An investigation on the behaviour and stiffness of reinforced concrete slabs subjected to torsion. *Materials Science and Engineering,* 164**,** 1-8.

NGUYEN, M., PHAM, P. & VUONG, N. 2016. An experimental study on torsional stiffness of reinforced concrete slab. *7th International Conference of Asian Concrete Federation.* Vietnam.

NILSON, A., DARWIN, D. & DOLAN, C. 2010. *Design of Concrete Structure,* New York, McGraw-Hill Companies.

PENG, X. & WONG, Y. 2011. Behavior of reinforced concrete walls subjected to monotonic pure torsion- An experimental study. *Engineering Structures,* 33**,** 2495-2508.

SAENZ, L. P. 1964. Equation for the stress-strain curve of concrete. *ACIJour,* 61**,** 1229-1235.

TAMAI, S. 1988. Average stress-strain relationship in post yield range of steel bar in concrete. *Concrete Lib JSCE,* 11**,** 117-129.

WANG, T. & HSU, T. 2001. Nonlinear finite element analysis of concrete structures using new constitutive models. *Comput Struct,* 79**,** 2781-2791.

YASEEN, S. & IHSAN, M. 2020. Finite element modeling of high strength self-compacting concrete T-beams under flexural load reinforced by ARFP. *ZANCO Journal of Pure and Applied Sciences,* 32**,** 176-184.